

Mass and energy balance calculations for an artificial ice reservoir (Icestupa)

Suryanarayanan Balasubramanian^{1,*}, Martin Hoelzle¹, Michael Lehning²,
Sonam Wangchuk³, Johannes Oerlemans⁴ and Felix Keller⁵

¹ University of Fribourg, Fribourg, Switzerland

² WSL Institute for Snow and Avalanche Research, Davos, Switzerland

³ Himalayan Institute of Alternatives Ladakh, Leh, India

⁴ Institute for Marine and Atmospheric Research, Utrecht University, Utrecht, The Netherlands

⁵ Academia Engiadina, Samedan, Switzerland

Correspondence*:

Suryanarayanan Balasubramanian

suryanarayanan.balasubramanian@unifr.ch

2 ABSTRACT

Artificial Ice Reservoirs (AIR) have been successful in storing water during winter and releasing the water during spring and summer. This has made them a reliable fresh water resource for irrigation in dry environments. Several AIRs have been built but studies of their water storage capacity and efficiency are scarce. This study attempts to model a cone-shaped AIR popularly called Icestupa. Important processes involved in the development and temporal evolution of an Icestupa are calculated by a physically-based model using equations governing the heat transfer, vapour diffusion and water transport of a phase changing water mass. These processes were quantified using meteorological data in conjunction with fountain spray information (mass input of an Icestupa) to estimate the quantity of frozen, melted, evaporated and drained water at a location called 'Eispalast' in the Schwarzsee region in the Canton of Fribourg, Switzerland. At this measurement site, an Icestupa was built for model validation purposes. The model was further tested by performing sensitivity and uncertainty study showing that the most sensitive parameters are the temperature threshold used to determine precipitation phase and the ice emissivity. Model calculations estimate that the Schwarzsee Icestupa only stored about 8% of the total water sprayed as ice. In addition, we found that reducing nozzle diameter of the fountain to 3 mm increases the storage efficiency up to 93% without compromising on the storage duration.

Keywords: iceslupa, mass balance, water storage, climate change adaptation, geoengineering

1 INTRODUCTION

Seasonal snow cover, glaciers and permafrost are expected to change their water storage capacity due to climate change with major consequences for downriver water supply (Immerzeel et al., 2019). The challenges brought about by these changes are especially important for dry mountain environments such as in Central Asia or the Andes, which directly rely on the seasonal meltwater for their farming and drinking needs (Hoelzle et al., 2019; Apel et al., 2018; Buytaert et al., 2017; Chen et al., 2016; Unger-Shayesteh



Figure 1. Icestupa in Ladakh, India on March 2017 was 24 m tall and contained around 3.7 million litres of water. Picture Credits: Lobzang Dadul

25 et al., 2013). Some villages in Ladakh, India have already been forced to relocate due to glacial retreat and
26 the corresponding loss of their main fresh water resources (Grossman, 2015).

27 Artificial Ice Reservoirs (AIR) have been considered to be a feasible way to adapt to these changes
28 (Hock et al., 2019; Nüsser et al., 2019b). An artificial ice reservoir is a human-made ice structure typically
29 constructed during the cold winter months and designed to slowly release freshwater during the warm and
30 dry spring and summer months. The main purpose of AIR is irrigation. Therefore, AIRs are designed to
31 store water in the form of ice as long into the summer as possible. The energy required to construct an AIR
32 is usually derived from the gravitational head of the source water body. Some are constructed horizontally
33 by freezing water using a series of checkdams and others are built vertically by spraying water through
34 fountain systems (Nüsser et al., 2019a). The latter are colloquially referred to as Icestupas and are the
35 subject of this study.

36 Since their invention in 2013 (Wangchuk, 2014), Icestupas have gained widespread publicity in the region
37 of Ladakh, Northern India since they require very little infrastructure, skills and energy to be constructed
38 in comparison to other water storage technologies. Compared to other AIR geometries, Icestupas (Fig.
39 1) can be built at lower altitudes and last much longer into the summer than other types of ice structures
40 (Wangchuk, 2014).

41 A typical Icestupa just requires a pipeline attached to a vertically mounted metal pipe with a fountain
42 nozzle for construction. Water source is usually a high altitude lake or glacial stream. Due to the altitude
43 difference between the pipeline input and fountain output, water ejects from the fountain nozzle as droplets
44 that eventually lose their latent heat to the atmosphere and accumulate as ice around the metal pipe.
45 The fountain nozzle is raised through addition of further pipes as and when significant ice accumulates.
46 Typically, a dome of branches is constructed around the metal pipe so that such pipe extensions can be
47 done from within this dome. During the winter, the fountain is manually activated between sunset and
48 sunrise. Threads, tree branches and fishing nets are used to guide and accelerate the ice formation.

49 If AIR are to become a viable water resource management tool, it is crucial to be able to propose suitable
50 construction sites, and to identify and minimize water losses. However, to date, no reliable estimates exist
51 about the amount of sprayed water that is necessary to create them and the meltwater they provide (Nüsser

et al., 2019a). Rough estimates of Icestupa meltwater in Ladakh suggest that the water loss during the construction process is considerable (see Appendix 8.1). A complete set of measurements of the water storage and energy balance are urgently required to understand the cause of the water losses better and increase the construction efficiency.

In this paper, we aim to develop a physically-based model of a vertical AIR (or Icestupa) that can quantify their storage efficiency using existing weather and water usage information. Mass and energy balance equations were used to estimate the quantity of water frozen, melted, evaporated and wasted. Sensitivity and uncertainty analysis were performed to identify the most critical parameters and the variance caused by them. For validation, we created an Icestupa at an accessible site (called Eispalast) near Schwarzsee in the Canton of Fribourg, Switzerland, allowing easy maintenance and control of the measurements. Due to the low altitude of the site with relatively high winter temperatures, only a small Icestupa could be established during winter 2018/19 for providing us with model validation data. Our model and validation experiments provide first steps towards evaluating the effectiveness of a vertical AIR for irrigation and finally we outline some preliminary guidelines for consideration when a construction of an Icestupa for water storage is envisaged.

2 STUDY SITE

The 'Eispalast' site in the Schwarzsee region lies at 967 m a.s.l. In the winter (Oct-Mar), mean daily maximum and minimum air temperatures vary between 14 to -4 °C. Clear skies are rare, averaging around 7 days, and precipitation amounts average 155 mm per month during winter (Meteoblue, 2020). The site was situated adjacent to a stream resulting in high humidity values across the study period. Within the 'Eispalast' site, 1.8 m in radius enclosure was constructed for the experiment. An automatic weather station (AWS) was set in place adjacent to the wooden boundary as shown in Fig. 2. The fountain used for spraying water had a nozzle diameter of 5 mm and a height of 1.35 m, and was placed in the centre of the wooden enclosure. The water was transferred from a spring water source at 1267 m a.s.l. by pipeline and flowed via a flowmeter and an air escape valve to the nozzle, where it was sprinkled with a spray radius of around 1.7 m. The air escape valve was installed to avoid errors in the flow measurements due to air bubbles. In addition, a webcam guaranteed a continuous survey of the site during the construction of the Icestupa.

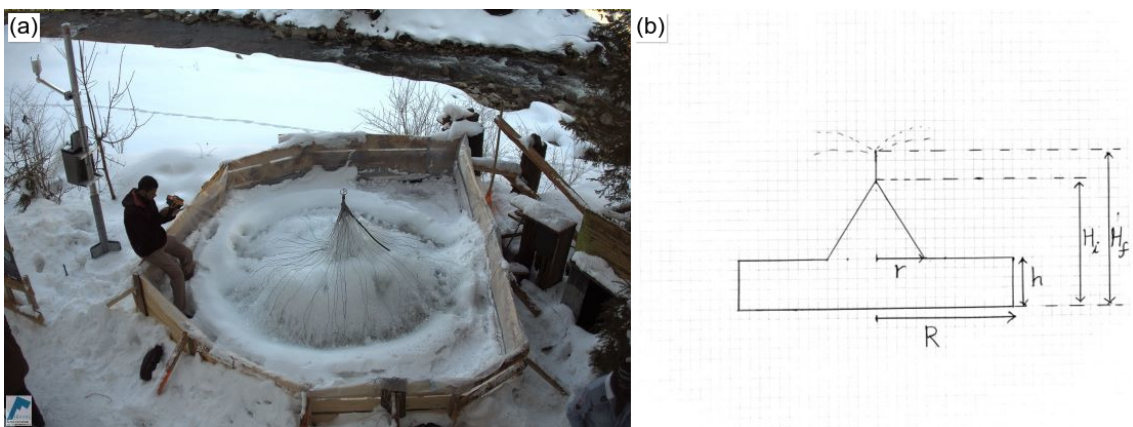


Figure 2. (a) The ice structure during the first validation measurement as seen on the webcam image of 14th Feb. (b) The corresponding cross section of the Schwarzsee ice structure with the field estimates of r , R , h , H_i , H_f used to determine the Icestupa volume is shown on the right.

78 **2.1 Construction**

79 From 30th January to 18th March 2019 the Icestupa was constructed through the fountain spray, which
 80 was manually switched on if measured air temperature was below -5 °C after sunset and was switched
 81 off as soon as the ice was exposed to daylight or temperatures were above 0 °C. The water spray of the
 82 fountain was initially adjusted so that most of the water droplets land within the wooden boundary zone.
 83 The ice formation was guided by adding a metal framework at the ice structure base after the first night of
 84 operation. Several cotton threads were tied between the ice structure base and fountain pole for accelerating
 85 and further guiding the ice formation process.

86 **2.2 Measurements and Data**

87 The Schwarzsee AWS was located at 967 m a.s.l. It was in operation from 30th January to 18th March
 88 2019. Measurements comprise air temperature, relative humidity, water flow, wind speed and direction.
 89 All these measurements were stored as 5 minute means. Precipitation data was derived from the Plaffeien
 90 AWS (IDAWEB, 2019) located 8.8 km away from the measurement site at an altitude of 1042 m a.s.l.

91 ERA5 reanalysis dataset (Copernicus Climate Change Service (C3S), 2017) was used to obtain the rest of
 92 the meteorological parameters namely the global and diffuse shortwave radiation and the cloudiness index.
 93 ERA5 surface solar radiation downwards parameter was used as a proxy for global radiation and total sky
 94 direct solar radiation parameter was subtracted from it to derive the diffuse radiation. Total cloud cover
 95 parameter of ERA5 represented the cloudiness index. The hourly ERA5 data and the 10 minute Plaffeien
 96 AWS data were linearly interpolated to the 5 minute data frequency of the Schwarzsee AWS.

97 Due to a power failure, all data from the Schwarzsee AWS was lost between 27th February 15:20 to 2nd
 98 March 15:00. Consequently, the amount of missing data in the dataset was around 6.7%. During heavy
 99 snowfall events, the ultrasonic wind sensor was blocked and recorded zero values. These data gaps and
 100 errors were filled with the ERA5 reanalysis dataset. ERA5 dataset is produced at a 1-hourly time step.
 101 Its horizontal resolution is approximately 30 km and it computes atmospheric variables at 137 pressure
 102 levels (Hersbach et al., 2020). The ERA5 grid point chosen(Latitude 46.640, Longitude 7.240) for the
 103 Schwarzsee site was around 9 km away from the actual site. So in order to fit the corresponding variables
 104 in the Schwarze dataset, the following modifications on the ERA5 parameters were necessary:

- 105 • Air temperature: This variable correlated well ($r^2 = 0.73$) with 2m temperature of ERA5. It was
 106 further corrected using the following equation:

$$f_{corr}(x, y) = y + sgn(rmse(x, y)) \cdot rmse(x, y) \quad (1)$$

where f_{corr} was the correction function used, x was the Schwarzsee temperature dataset (T_{SZ}), y was the ERA5 temperature dataset (T_{ERA5}), sgn is the signum function and $rmse$ was the root mean square error function defined as:

$$rmse(x, y) = \sqrt{\left(\frac{1}{n}\right) \sum_{i=1}^n (y_i - x_i)^2}$$

- 107 • Relative Humidity: Near-surface humidity is not archived directly in ERA datasets, but from near-
 108 surface (2m from the surface) temperature (T_{ERA5}) and dew point temperature (Td_{ERA5}) one can

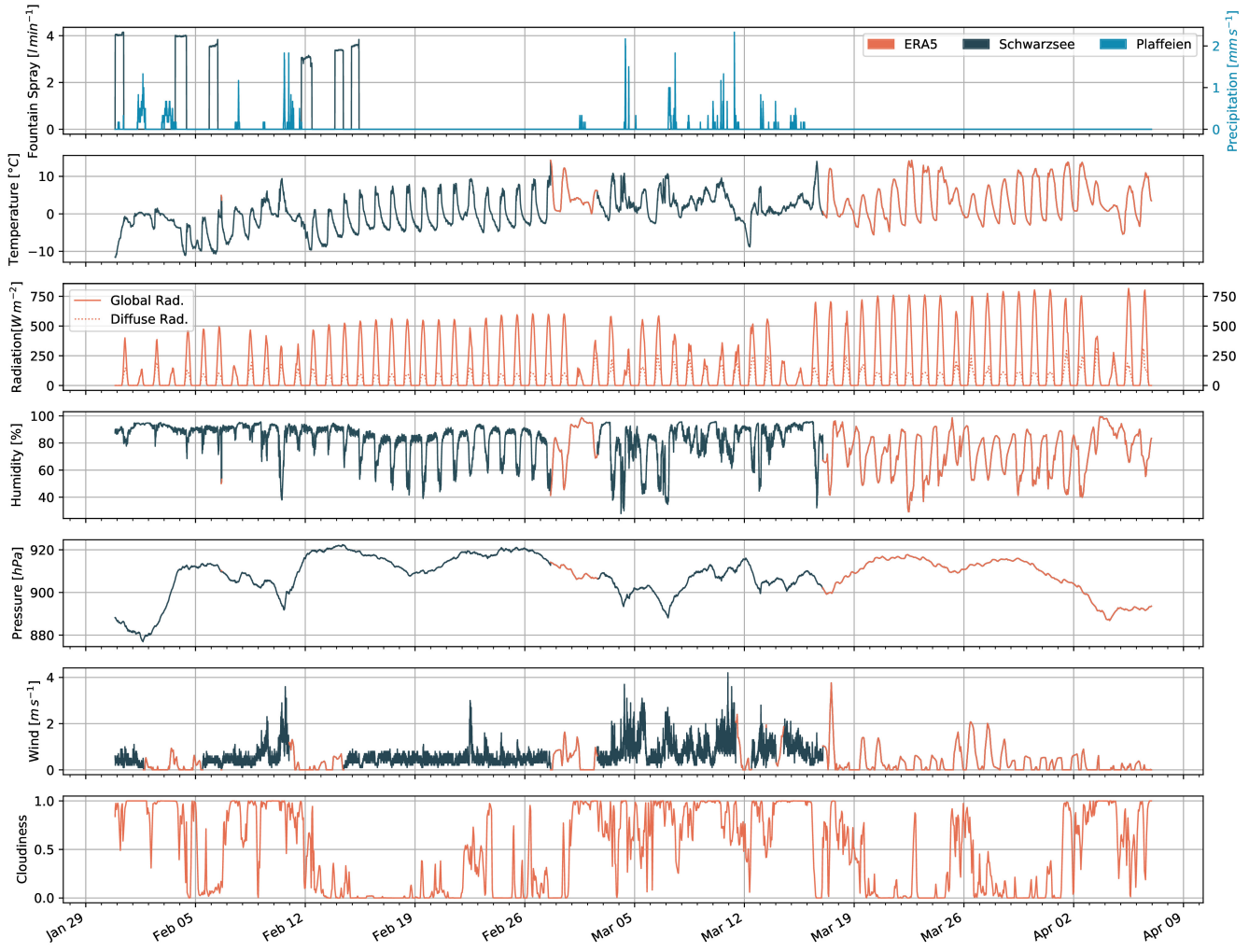


Figure 3. Measurements at the AWS of Schwarzsee (black) were used as main model input data in 5 minute frequency. Plaffeien AWS (blue) provided the precipitation data. Cloudiness and incoming shortwave radiation were obtained from the ERA5 reanalysis dataset (orange).

109 calculate relative humidity(RH) at 2m as follows:

$$RH = 100 \cdot \frac{e_{sat}(T_{dERA5})}{e_{sat}(T_{ERA5})} \quad (2)$$

110 where the saturation vapour pressure function e_{sat} is expressed with the Teten's formula (Tetens, 1930):

$$e_{sat}(T) = a_1 \cdot e^{(a_3 \cdot \frac{T}{(T+273.16-a_4)})} \quad (3)$$

111 with T in $^{\circ}C$ and the parameters set for saturation over water ($a_1 = 611.21$ Pa, $a_3 = 17.502$ and $a_4 = 32.19$ K) according to Buck (1981). This derived variable was poorly correlated ($r^2 = 0.38$) with the Schwarzsee measurements.

- 114 • Air Pressure: This variable correlated well ($r^2 = 0.99$) with surface pressure of ERA5. It was further
115 modified using the correction function f_{corr} .

116 • Wind Speed: This variable correlated poorly ($r^2 = 0.49$) with 10m wind speed of ERA5. We applied
 117 the f_{corr} function to better fit ERA5 to Schwarzsee. There was another cause of missing wind speed
 118 data as the ultrasonic wind sensor recorded zero wind speed values due to snow accumulation on it. So
 119 all zero wind speed values were also replaced with the corrected ERA5 data.

120 Through this modified ERA5 dataset, we were also able to further extend the Schwarzsee dataset and
 121 allow the model to run beyond 18th March 2019. Precipitation was filled as null values beyond 18th March
 122 2019.

123 2.2.1 Field Measurements for validation

124 Estimates of the ice volumes were obtained by two manual measurements of the ice structure dimensions.
 125 The first corresponds to the end of the freezing period on 14th February 16:00 (only one more fountain
 126 run was possible after this date). The second corresponds to the end of the melting process on 10th March
 127 18:00. The field validations are shown by green lines in Fig. 8.

128 On 14th February the ice volume was calculated using a simplistic cross section of the structure as shown
 129 in Fig. 2. We used the following field estimates of r , R , h , H_i , H_f (see Fig. 2 for the different geometry
 130 components) to determine the maximum and minimum volumes:

$$0.55 \leq r \leq 1m ; 1.1 \leq R \leq 1.2m ; 0.1 \leq h \leq 0.2m ; 0.6 \leq H_i \leq 0.8m ; 1.3 \leq H_f \leq 1.4m \quad (4)$$

131 The second validation point was considered to be on March 10th 18:00. Based on the webcam imagery
 132 and manual measurement, a thin layer of ice with an observed thickness between 0.01 to 0.06 m could be
 133 quantified. This results in an ice volume estimate for the first validation date on 14th February 2019 to be
 134 $0.857 \pm 0.186 m^3$ and for the second validation date on 11th March 2019 to be $0.13 \pm 0.09 m^3$.

135 In reality, the Schwarzsee ice structure was more cylindrical until a height of 0.2 m and conical afterwards
 136 until a height of 0.6 m with a radius of 1.18 m. However, we assume a conical shape of this ice structure in
 137 order to apply the modelling strategy described below.

3 MODEL SETUP

138 The model (implemented in python) consists of three parts calculating a) the geometric evolution of the
 139 Icestupa, b) the energy balance and c) the mass balance as shown schematically in Fig. 4. A bulk energy
 140 and mass balance model is used to calculate the amounts of ice, liquid water, water vapour and drained
 141 water of the Icestupa every 5 minutes. The equations used henceforth display model time step superscript
 142 only if it is different from the current time step.

143 3.1 Icestupa geometric evolution

144 Radius r_{ice} and height h_{ice} define the dimensions of the Icestupa assuming its geometry to be a cone as
 145 shown in Fig. 5. The surface area A and volume V exposed to the atmosphere are:

$$A = \pi \cdot r_{ice} \cdot \sqrt{r_{ice}^2 + h_{ice}^2} \quad (5)$$

$$V = \pi/3 \cdot r_{ice}^2 \cdot h_{ice} \quad (6)$$

146 With the mass of the Icestupa M_{ice} , its current volume can also be expressed as:

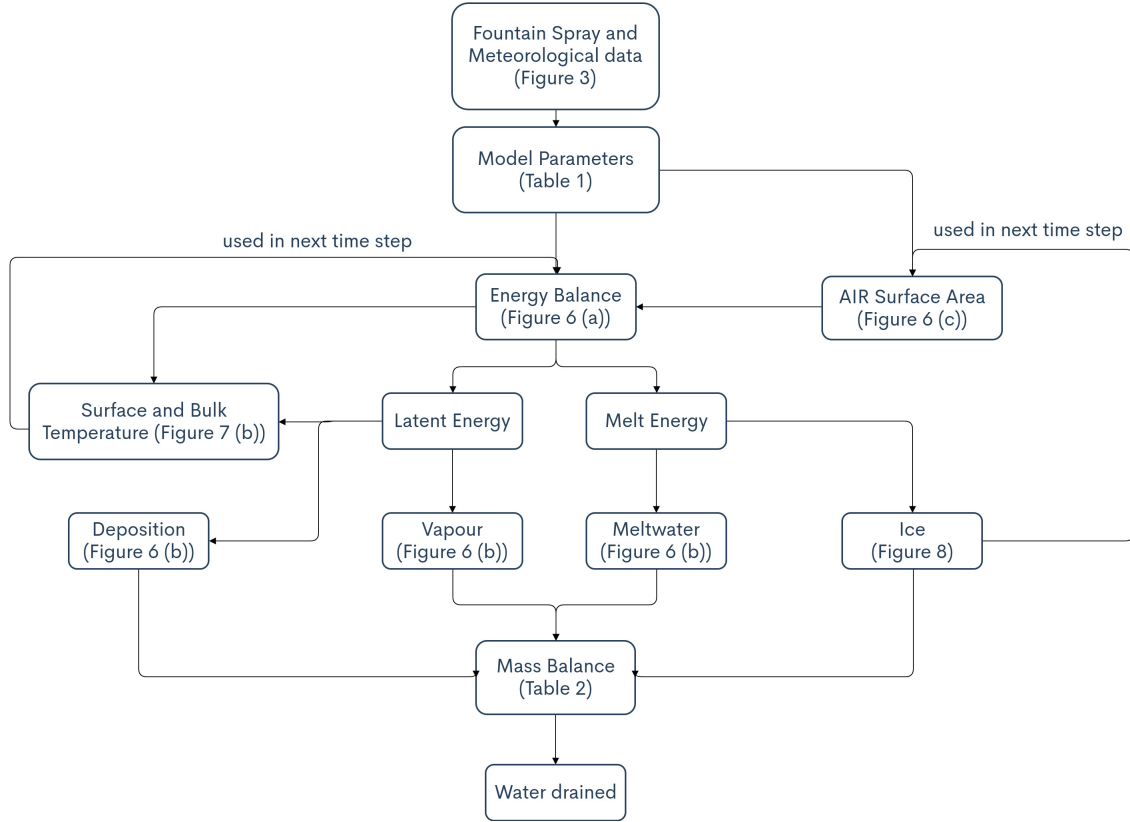


Figure 4. Model schematic showing the algorithm used in the model at every time step. Further details about these variables can be found in the associated tables and figures.

$$V = M_{ice}/\rho_{ice} \quad (7)$$

147 where ρ_{ice} is the density of ice (917 kg m^{-3}). The model of the Icestupa is initialised with a thickness
 148 of Δx (defined in 3.2) and a circular area of radius r_F . The constant r_F represents the mean spray radius
 149 of the fountain. This fountain spray radius is determined by modelling the projectile motion of the water
 150 droplets. Using mass conservation the droplet speed v_F can be determined from the spray rate d_F and the
 151 diameter dia_F of the nozzle as follows:

$$v_F = \frac{d_F}{\pi \cdot dia_F^2/4} \quad (8)$$

152 Afterwards, we assume that the water droplets move with an air friction free projectile motion from
 153 the fountain nozzle with a height h_F to the ice/ground surface. The resulting spray radius r_F was then
 154 determined from the projectile motion equation as follows:

$$r_F = \frac{v_F \cdot \cos\theta_F (v_F \cdot \sin\theta_F + \sqrt{(v_F \cdot \sin\theta_F)^2 + 2 \cdot g \cdot h_F})}{g} \quad (9)$$

155 where $g = 9.8 \text{ ms}^{-2}$ is the acceleration due to gravity and $\theta_F = 45^\circ$ is the angle of launch.

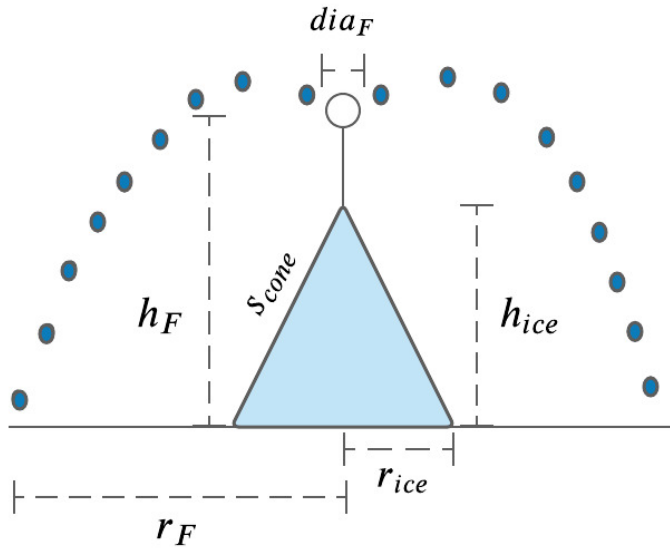


Figure 5. Shape and fountain parameters of the Schwarzsee Icestupa. r_{ice} is the radius, h_{ice} is the height and s_{cone} is the slope of the ice cone. r_F is the spray radius, h_F is the height and dia_F is the nozzle diameter of the fountain.

156 During subsequent time steps, the dimensions of the Icestupa evolve assuming a uniform ice formation
 157 and decay across its surface area with an invariant slope $s_{cone} = \frac{h_{ice}}{r_{ice}}$ as shown in Fig. 5. During these time
 158 steps, the volume is parameterised using Eqn. 6 as:

$$V = \pi/3 \cdot r_{ice}^3 \cdot s_{cone} \quad (10)$$

159 However, the Icestupa cannot outgrow the maximum range of the water droplets ($(r_{ice})_{max} = r_F$).
 160 Combining equations 6, 7 and 10, the geometric evolution of the Icestupa at each time step i can be
 161 determined by considering the following rules:

$$(r_{ice}, h_{ice}) = \begin{cases} (r_F, \Delta x) & \text{if } i = 0 \\ (r_{ice}^{i-1}, \frac{3 \cdot M_{ice}}{\pi \cdot \rho_{ice} \cdot (r_{ice}^{i-1})^2}) & \text{if } r_{ice}^{i-1} \geq r_F \text{ and } \Delta M_{ice} > 0 \text{ where } \Delta M_{ice} = M_{ice}^{i-1} - M_{ice}^{i-2} \\ (\frac{3 \cdot M_{ice}}{\pi \cdot \rho_{ice} \cdot s_{cone}})^{1/3} \cdot (1, s_{cone}) & \text{otherwise} \end{cases} \quad (11)$$

162 3.2 Energy Balance

163 The energy balance equation for the Icestupa is formulated as follows:

$$q_{net} = q_{SW} + q_{LW} + q_L + q_S + q_F + q_G \quad (12)$$

164 where q_{net} is the net energy flux in $[W m^{-2}]$; q_{SW} is the net shortwave radiation; q_{LW} is the net longwave
 165 radiation; q_L and q_S are the turbulent latent and sensible heat fluxes. q_F represents the heat exchange
 166 created due to the additional water and ice boundary present during fountain on time steps. q_G represents
 167 ground heat flux between Icestupa surface and Icestupa interior. Energy transferred in the direction of the
 168 ice surface is always denoted as positive and away as negative. Also, all temperature variables are assigned
 169 in units of $[^\circ C]$.

170 Equation 12 is usually referred to as the energy budget for “the surface”, but practically it must apply to a
 171 surface layer of ice with a finite thickness Δx . The energy flux acts upon the Icestupa surface layer which
 172 has an upper and a lower boundary defined by the atmosphere and the ice body of the Icestupa, respectively.
 173 The parameter selection for Δx is based on the following two arguments: (a) the ice thickness Δx should
 174 be small enough to represent the daily surface temperature variations and (b) Δx should be large enough
 175 for these temperature variations to not reach the bottom of the surface layer. Therefore, we introduced a 5
 176 mm thick ice surface layer, over which the energy balance is calculated. A sensitivity analysis was later
 177 performed to understand the influence of this factor. Here, we define the surface temperature T_{ice} to be
 178 the modelled average temperature of the Icestupa surface layer and the energy flux q_{net} is assumed to act
 179 uniformly across the Icestupa area A .

180 3.2.1 Net Shortwave Radiation q_{SW}

181 The net shortwave radiation q_{SW} is computed as follows:

$$q_{SW} = (1 - \alpha) \cdot (SW_{direct} \cdot f_{cone} + SW_{diffuse}) \quad (13)$$

182 where $SW_{direct} = SW_{global} - SW_{diffuse}$ with the measured global and diffuse short wave radiation as
 183 SW_{global} and $SW_{diffuse}$, the modelled albedo as α and with f_{cone} as the area fraction of the ice structure
 184 exposed to the direct shortwave radiation.

185 We model the albedo using a scheme described in Oerlemans and Knap (1998). The scheme records the
 186 decay of albedo with time after fresh snow is deposited on the surface. δt records the number of time steps
 187 after the last snowfall event. After snowfall, albedo changes over a time step, δt , as

$$\alpha = \alpha_{ice} + (\alpha_{snow} - \alpha_{ice}) \cdot e^{(-\delta t)/\tau} \quad (14)$$

188 where α_{ice} is the bare ice albedo value and τ is a decay rate, which determines how fast the albedo of the
 189 ageing snow reaches this value. The decay rate τ is assumed to have a base value of 10 days similar to
 190 values obtained by Schmidt et al. (2017) for wet surfaces and its maximal value is set based on observations
 191 by Oerlemans and Knap (1998) as shown in Table 1. Furthermore, the albedo α varies depending on the
 192 water source that formed the current Icestupa surface. Correspondingly, the albedo is reset to the value
 193 of bare ice albedo if the fountain is spraying water onto the current ice surface and to the value of fresh
 194 snow albedo if a snowfall event occurred. Snowfall events are assumed if the air temperature is below
 195 $T_{rain} = 1^\circ C$.

196 The area fraction f_{cone} of the ice structure exposed to the direct shortwave radiation depends on the
 197 shape considered. This factor is derived by calculating the area influenced by the vertical and horizontal
 198 components of the direct solar radiation. For a conical shape, half of the total curved surface is exposed to
 199 the vertical component of the direct shortwave radiation and the projected triangle of the curved surface
 200 is exposed to the horizontal component of the direct shortwave radiation. The solar elevation angle θ_{sun}
 201 used is modelled using the parametrisation proposed by Woolf (1968). Accordingly, f_{cone} is determined as
 202 follows:

$$f_{cone} = \frac{(0.5 \cdot r_{ice} \cdot h_{ice}) \cdot \cos\theta_{sun} + (\pi \cdot r_{ice}^2 / 2) \cdot \sin\theta_{sun}}{\pi \cdot r_{ice} \cdot (r_{ice}^2 + h_{ice}^2)^{1/2}} \quad (15)$$

203 The measured diffuse shortwave radiation is assumed to impact the conical Icestupa surface uniformly.

204 3.2.2 Net Longwave Radiation q_{LW}

205 The net longwave radiation q_{LW} , for which there were no direct measurements available at Schwarzsee,
 206 is determined as follows:

$$q_{LW} = \sigma \cdot (\epsilon_a \cdot (T_a + 273.15)^4 - \epsilon_{ice} \cdot (T_{ice} + 273.15)^4) \quad (16)$$

207 where T_a represents the measured air temperature, T_{ice} is the modelled surface temperature, both
 208 temperatures are given in $^\circ C$, $\sigma = 5.67 \cdot 10^8$ is the Stefan-Boltzmann constant, ϵ_a denotes the atmospheric
 209 emissivity and ϵ_{ice} is the corresponding emissivity value for the Icestupa surface (see Table 1).

210 For the calculation of the incoming longwave radiation, we approximate atmospheric emissivity ϵ_a using
 211 the equation suggested by Brutsaert (1982), considering air temperature and vapor pressure (Eqn. 18). The
 212 vapor pressures over air and ice was obtained using the following formulation given in WMO (2018):

$$\begin{aligned} p_{v,a} &= 6.107 \cdot 10^{(7.5 \cdot T_a / (T_a + 237.3))} \\ p_{v,ice} &= (1.0016 + 3.15 \cdot 10^{-6} \cdot p_a - 0.074 \cdot p_a^{-1}) \cdot (6.112 \cdot e^{(22.46 \cdot T_{ice} / (T_{ice} + 272.62))}) \end{aligned} \quad (17)$$

213 where $p_{v,a}$ denotes the saturation vapor pressure of air, $p_{v,ice}$ denotes the saturation vapor pressure of ice
 214 and p_a is the measured air pressure in $[hPa]$. The expression defined in Brutsaert (1975) for clear skies
 215 (first term in equation 18) is extended with the correction for cloudy skies after Brutsaert (1982) as follows:

$$\epsilon_a = 1.24 \cdot \left(\frac{p_{v,a}}{(T_a + 273.15)} \right)^{1/7} \cdot (1 + 0.22 \cdot c^2) \quad (18)$$

216 with a cloudiness index c , ranging from 0 for clear skies to 1 for complete overcast skies, obtained from
 217 the ERA5 reanalysis data as shown in Fig. 3.

218 3.2.3 Turbulent sensible q_S and latent q_L heat fluxes

219 The turbulent sensible q_S and latent heat q_L fluxes are computed with the following expressions proposed
 220 by Garratt (1992):

$$q_S = c_a \cdot \rho_a \cdot p_a / p_{0,a} \cdot \frac{\kappa^2 \cdot v_a \cdot (T_a - T_{ice})}{\left(\ln \frac{h_{AWS}}{z_{ice}} \right)^2} \quad (19)$$

$$q_L = \begin{cases} 0.623 \cdot L_s \cdot \rho_a / p_{0,a} \cdot \frac{\kappa^2 \cdot v_a (p_{v,a} - p_{v,ice})}{\left(\ln \frac{h_{AWS}}{z_{ice}} \right)^2} & \text{if } \Delta M_F = 0 \\ 0 & \text{if } \Delta M_F > 0 \text{ where } \Delta M_F = M_F^i - M_F^{i-1} \end{cases} \quad (20)$$

221 where h_{AWS} is the measurement height above the ground surface of the AWS (in m), v_a is the wind
 222 speed in [$m s^{-1}$] and M_F denotes fountain water spray mass in [kg]. c_a is the specific heat of air at constant
 223 pressure ($1010 \text{ J kg}^{-1} \text{ K}^{-1}$), ρ_a is the air density at standard sea level (1.29 kg m^{-3}), $p_{0,a}$ is the air pressure
 224 at standard sea level (1013 hPa), κ is the von Karman constant (0.4), L_s is the heat of sublimation (2848
 225 $kJ kg^{-1}$) and z_{ice} (1.7 mm) denotes the roughness length of ice (momentum and scalar).

226 3.2.4 Fountain water heat flux q_F

227 The total energy flux is further influenced through the heat flux caused by the water that was additionally
 228 added to the surface of the Icestupa during the time the fountain was running. We take this interaction
 229 between the fountain water and the ice surface into account by assuming that the ice surface temperature
 230 stays constantly at $0^\circ C$ during time steps when the fountain is active. This process can be divided into two
 231 simultaneous steps: (a) the water temperature T_{water} is cooled to $0^\circ C$ and (b) the ice surface temperature is
 232 warmed to $0^\circ C$. Process (a) transfers hereby the necessary energy for process (b) throughout the fountain
 233 runtime. We further assume that this process is instantaneous, i.e. the ice temperature is immediately set
 234 to $0^\circ C$ within just one time step Δt when the fountain is switched on. Thus, the heat flux caused by the
 235 fountain water is calculated as follows:

$$q_F = \begin{cases} 0 & \text{if } \Delta M_F = 0 \\ \frac{\Delta M_F \cdot c_{water} \cdot T_{water}}{\Delta t \cdot A} + \frac{\rho_{ice} \cdot \Delta x \cdot c_{ice} \cdot T_{ice}}{\Delta t} & \text{if } \Delta M_F > 0 \end{cases} \quad (21)$$

236 with c_{ice} as the specific heat of ice.

237 3.2.5 Bulk Icestupa heat flux q_G

238 The bulk Icestupa heat flux q_G corresponds to the ground heat flux in normal soils and is caused by
 239 the temperature gradient between the surface layer and the ice body. It is expressed by using the heat
 240 conduction equation as follows:

$$q_G = k_{ice} \cdot (T_{bulk} - T_{ice}) / l_{ice} \quad (22)$$

241 where k_{ice} is the thermal conductivity of ice in $[W\ m^{-1}\ K^{-1}]$, T_{bulk} is the mean temperature of the ice
 242 body within the Icestupa and l_{ice} is the average distance of any point in the surface to any other point in the
 243 ice body. T_{bulk} is initialised as $0\ ^\circ C$ and later determined from Eqn. 22 as follows:

$$T_{bulk} = T_{bulk}^{i-1} - (q_G \cdot A \cdot \Delta t) / (M_{ice} \cdot c_{ice}) \quad (23)$$

244 Since we assume a conical shape with $r_{ice} > h_{ice}$, l_{ice} cannot be greater than $2r_{ice}$ and also cannot
 245 be less than Δx . Therefore, the average distance from any point on the surface to any point inside is
 246 $\Delta x \leq l_{ice} \leq r_{ice}$. We calculate q_G here assuming $l_{ice} = r_{ice}/2$.

247 3.2.6 Surface temperature changes and melt energy q_{melt}

248 The available net energy q_{net} partly increases surface temperature, but also contributes to ice melt at the
 249 surface of the Icestupa. q_T denotes the energy used on changing the surface temperature T_{ice} and q_{melt}
 250 denotes the energy used to produce meltwater. So Eqn. 12 can be rewritten as:

$$q_{net} = q_{melt} + q_T \quad (24)$$

251 The temperature fluctuates based on 3 scenarios namely, (1) the energy flux is negative but cannot freeze
 252 all the fountain water output; (2) the energy flux is negative and can freeze all the fountain water output and
 253 (3) the fountain is inactive ($\Delta M_F = 0$). Also, the latent heat always contributes to temperature fluctuations.
 254 Therefore, we express the rate of change of temperature as follows:

$$\frac{\Delta T}{\Delta t} = \begin{cases} -T_{ice}^{i-1} / \Delta t & \text{if } (q_{net} - q_L) < 0 \text{ and } \Delta M_F \geq -(q_{net} - q_L) \cdot A \cdot \Delta t / L_f \\ (\Delta M_F \cdot L_f) / (\rho_{ice} \cdot c_{ice} \cdot \Delta x \cdot A \cdot \Delta t) & \text{if } (q_{net} - q_L) < 0 \text{ and } \Delta M_F < -(q_{net} - q_L) \cdot A \cdot \Delta t / L_f \\ q_{net} / (\rho_{ice} \cdot c_{ice} \cdot \Delta x) & \text{if } \Delta M_F = 0 \end{cases} \quad (25)$$

255 Whenever the model predicts $T_{ice}^{i+1} > 0^\circ C$, then the surface temperature is set to $0^\circ C$ in the corresponding
 256 time step and additional energy contributes to q_{melt} . Combining these requirements, we get:

$$(q_T, q_{melt}) = \begin{cases} (\rho_{ice} \cdot c_{ice} \cdot \Delta x \cdot \frac{\Delta T}{\Delta t}, q_{net} - q_L - \rho_{ice} \cdot c_{ice} \cdot \Delta x \cdot \frac{\Delta T}{\Delta t}) & \text{if } T_{ice}^{i+1} \leq 0^\circ C \text{ and } \Delta M_F > 0 \\ (\rho_{ice} \cdot c_{ice} \cdot \Delta x \cdot \frac{\Delta T}{\Delta t}, q_{net} - \rho_{ice} \cdot c_{ice} \cdot \Delta x \cdot \frac{\Delta T}{\Delta t}) & \text{if } T_{ice}^{i+1} \leq 0^\circ C \text{ and } \Delta M_F = 0 \\ (-\rho_{ice} \cdot c_{ice} \cdot \Delta x \cdot \frac{T_{ice}^i}{\Delta t}, q_{net} - q_L + \rho_{ice} \cdot c_{ice} \cdot \Delta x \cdot \frac{T_{ice}^i}{\Delta t}) & \text{if } T_{ice}^{i+1} > 0^\circ C \text{ and } \Delta M_F > 0 \\ (-\rho_{ice} \cdot c_{ice} \cdot \Delta x \cdot \frac{T_{ice}^i}{\Delta t}, q_{net} + \rho_{ice} \cdot c_{ice} \cdot \Delta x \cdot \frac{T_{ice}^i}{\Delta t}) & \text{if } T_{ice}^{i+1} > 0^\circ C \text{ and } \Delta M_F = 0 \end{cases} \quad (26)$$

Table 1. Free parameters in the model categorised as constant, uncertain and site parameters. Base value (B) and uncertainty (U) were taken from the literature. For assumptions (assum.), the uncertainty was chosen to be relatively large (5 %). For measurements (meas.), the uncertainty due to parallax errors is chosen to be (1 %).

Constant Parameters	Symbol	Value	Range	References
Van Karman constant	κ	0.4	n.a.	B: Cuffey and Paterson
Stefan Boltzmann constant	σ	$5.67 \cdot 10^{-8} W m^{-2} K^{-4}$	n.a.	B: Cuffey and Paterson
Air pressure at sea level	$p_{0,a}$	1013 hPa	n.a.	B: Mölg and Hardy
Density of water	ρ_w	$1000 kg m^{-3}$	n.a.	B: Cuffey and Paterson
Density of ice	ρ_{ice}	$917 kg m^{-3}$	n.a.	B: Cuffey and Paterson
Density of air	ρ_a	$1.29 kg m^{-3}$	n.a.	B: Mölg and Hardy
Specific heat of water	c_w	$4186 J kg^{-1} ^\circ C^{-1}$	n.a.	B: Cuffey and Paterson
Specific heat of ice	c_{ice}	$2097 J kg^{-1} ^\circ C^{-1}$	n.a.	B: Cuffey and Paterson
Specific heat of air	c_a	$1010 J kg^{-1} ^\circ C^{-1}$	n.a.	B: Mölg and Hardy
Thermal conductivity of ice	k_{ice}	$2.123 W m^{-1} K^{-1}$	n.a.	B: Bonales et al.
Latent Heat of Sublimation	L_s	$2848 kJ kg^{-1}$	n.a.	B: Cuffey and Paterson
Latent Heat of Evaporation	L_e	$2514 kJ kg^{-1}$	n.a.	B: Cuffey and Paterson
Latent Heat of Fusion	L_f	$334 kJ kg^{-1}$	n.a.	B: Cuffey and Paterson
Gravitational acceleration	g	$9.81 m s^{-2}$	n.a.	B: Cuffey and Paterson
Uncertain Parameters				
Precipitation	T_{rain}	$1 ^\circ C$	$\pm 1 ^\circ C$	B + U: Fujita and Ageta, Zhou et al.
Temperature threshold				
Ice Emissivity	ϵ_{ice}	0.95	$\pm 5 \%$	B: Cuffey and Paterson; U: assum.
Ice Albedo	α_{ice}	0.35	$\pm 5 \%$	B: Cuffey and Paterson; U: assum.
Snow Albedo	α_{snow}	0.85	$\pm 5 \%$	B: Cuffey and Paterson; U: assum.
Albedo Decay Rate	τ	10 days	$[1, 22] days$	B: Schmidt et al.; U: Oerlemans and Knap assum.
Ice layer thickness	Δx	5 mm	$[1, 10] mm$	
Site Parameters				
Fountain diameter	nozzle	dia_F	5 mm	$\pm 1 \%$ B: meas. ; U: assum.
Fountain Height		h_F	1.35 m	$\pm 1 \%$ B: meas. ; U: assum.
Fountain temperature	water	T_{water}	$5 ^\circ C$	$[0, 9] ^\circ C$ B: meas. ; U: meas.
AWS Height		h_{AWS}	3 m	$\pm 1 \%$ B: meas. ; U: assum.

$$M_F + M_{ppt} + M_{dpt} = M_{ice} + M_{melt} + M_{vapour} + M_{drained} \quad (27)$$

where M_F denotes the cumulative water input; M_{ppt} is the cumulative precipitation and M_{dpt} is the cumulative accumulation through water vapour condensation or deposition; M_{ice} is the cumulative mass of ice; M_{melt} is the cumulative mass of melt water; M_{vapour} represents the cumulative water vapor loss by evaporation or sublimation and $M_{drained}$ is the cumulative water that drains away.

Equation 27 can be rewritten using the mass balance change as:

$$\frac{\Delta M_F}{\Delta t} + \frac{\Delta M_{ppt}}{\Delta t} + \frac{\Delta M_{dpt}}{\Delta t} = \frac{\Delta M_{ice}}{\Delta t} + \frac{\Delta M_{melt}}{\Delta t} + \frac{\Delta M_{vapour}}{\Delta t} + \frac{\Delta M_{drained}}{\Delta t} \quad (28)$$

where $\Delta M = M^i - M^{i-1}$. Here $\frac{\Delta M_F}{\Delta t} = d_F$ where d_F is the spray of the fountain measured in $[kg\ s^{-1}]$. Precipitation input is calculated as:

$$\frac{\Delta M_{ppt}}{\Delta t} = \begin{cases} \pi \cdot r_{ice}^2 \cdot \rho_w \cdot ppt & \text{if } T_a < T_{rain} \\ 0 & \text{if } T_a \geq T_{rain} \end{cases} \quad (29)$$

where ρ_w is the density of water ($1000\ kg\ m^{-3}$), ppt is the measured precipitation rate in $[m\ s^{-1}]$ and T_{rain} is the temperature threshold below which precipitation falls as snow. Here, snowfall events were identified using T_{rain} as $1^{\circ}C$. Snow mass input is calculated by assuming a uniform deposition over the entire circular footprint of the Icestupa.

The latent heat flux is used to estimate either the evaporation and condensation processes or sublimation and deposition processes. Deposition and sublimation involve phase change between vapour and ice whereas evaporation and condensation involve phase change between meltwater and ice. To differentiate between these two possibilities, we classify the time steps into humid or non-humid if the corresponding relative humidity value is above or below 60 % (Stigter et al., 2018). On humid time steps we assume condensation or evaporation to occur whereas on non-humid time steps deposition or sublimation can occur. Correspondingly, latent heat of evaporation (L_e) is used for humid time steps and latent heat of sublimation (L_s) is used for non-humid time steps. Water accumulation and vapour loss from the Icestupa surface is calculated as follows:

$$\left(\frac{\Delta M_{vapour}}{\Delta t}, \frac{\Delta M_{dpt}}{\Delta t} \right) = \begin{cases} (-q_L \cdot A/L, 0) & \text{if } q_L < 0 \\ (0, q_L \cdot A/L) & \text{if } q_L \geq 0 \end{cases} \quad (30)$$

where $L = \begin{cases} L_e & \text{if } RH \geq 60 \\ L_s & \text{if } RH < 60 \end{cases}$

Using the melt energy q_{melt} , we estimate the frozen and melted ice mass (ΔM_{ice} , ΔM_{melt}). Removing the contribution of precipitation and combining Eqn. 30 we are left with the contribution from the melt energy as follows:

Table 2. Summary of calculated mass balance components for the Schwarzsee experiment after the fountain spray was stopped on 15th February and at the end of the model run on 1st April.

	Mass Component	Fountain spray ends	Model ends
Input	M_F	18060 kg	18060 kg
	M_{ppt}	439 kg	463 kg
	M_{dpt}	14 kg	62 kg
Output	M_{melt}	166 kg	1392 kg
	M_{ice}	1158 kg	0 kg
	M_{vapour} $M_{drained}$	4 kg 17184 kg	8 kg 17184 kg

$$\left(\frac{\Delta M_{ice} - \Delta M_{ppt} - \Delta M_{dpt} + \Delta M_{vapour}}{\Delta t}, \frac{\Delta M_{melt}}{\Delta t} \right) \begin{cases} \text{if } RH < 60 \\ \left(\frac{\Delta M_{ice} - \Delta M_{ppt} - \Delta M_{dpt}}{\Delta t}, \frac{\Delta M_{melt} + \Delta M_{vapour}}{\Delta t} \right) \begin{cases} \frac{q_{melt} \cdot A}{L_f} \cdot (-1, 1) & \text{if } q_{melt} \geq 0 \\ \frac{q_{melt} \cdot A}{L_f} \cdot (-1, 0) & \text{if } q_{melt} < 0 \text{ and } \frac{\Delta M_F}{\Delta t} \geq -q_{melt} \\ \left(\frac{\Delta M_F}{\Delta t}, 0 \right) & \text{if } q_{melt} < 0 \text{ and } 0 \leq \frac{\Delta M_F}{\Delta t} < -q_{melt} \end{cases} \end{cases} \quad (31)$$

281 Now, with all the other terms known in Eqn. 28, the water drained from the Icestupa can be expressed as:

$$\frac{\Delta M_{drained}}{\Delta t} = \frac{\Delta M_F + \Delta M_{ppt} + \Delta M_{dpt} - \Delta M_{ice} - \Delta M_{melt} - \Delta M_{vapour}}{\Delta t} \quad (32)$$

282 Considering AIR as water reservoirs, we can quantify their potential through the amount of water they
283 store (storage quantity) and the length of time they store it (storage duration). Another means of comparing
284 different Icestupas is through their water storage efficiency defined accordingly as:

$$\text{Storage Efficiency} = \frac{M_{melt}}{(M_F + M_{ppt} + M_{dpt})} \cdot 100 \quad (33)$$

4 MODEL RESULTS

285 The model was forced with meteorological data from 30th January to 1st April 2019 (Fig. 3) and various
286 parameters (see Table 1) to calculate the mass and energy balance of the Icestupa.

287 4.1 Energy and mass balance calculation

288 Daily averages of some components of the energy balance are shown in Fig. 6 (a). On average during the
289 experiment duration, the total energy flux between the atmosphere and the Icestupa are almost balanced.
290 Net shortwave radiation (28 W m^{-2}), sensible (17 W m^{-2}) and latent heat flux (9 W m^{-2}) with a mostly
291 positive flux towards the surface of the iceshelf are compensated by the net longwave radiation (- 36
292 W m^{-2}) and the melt energy (- 19 W m^{-2}). The contribution of other fluxes are negligible in comparison.

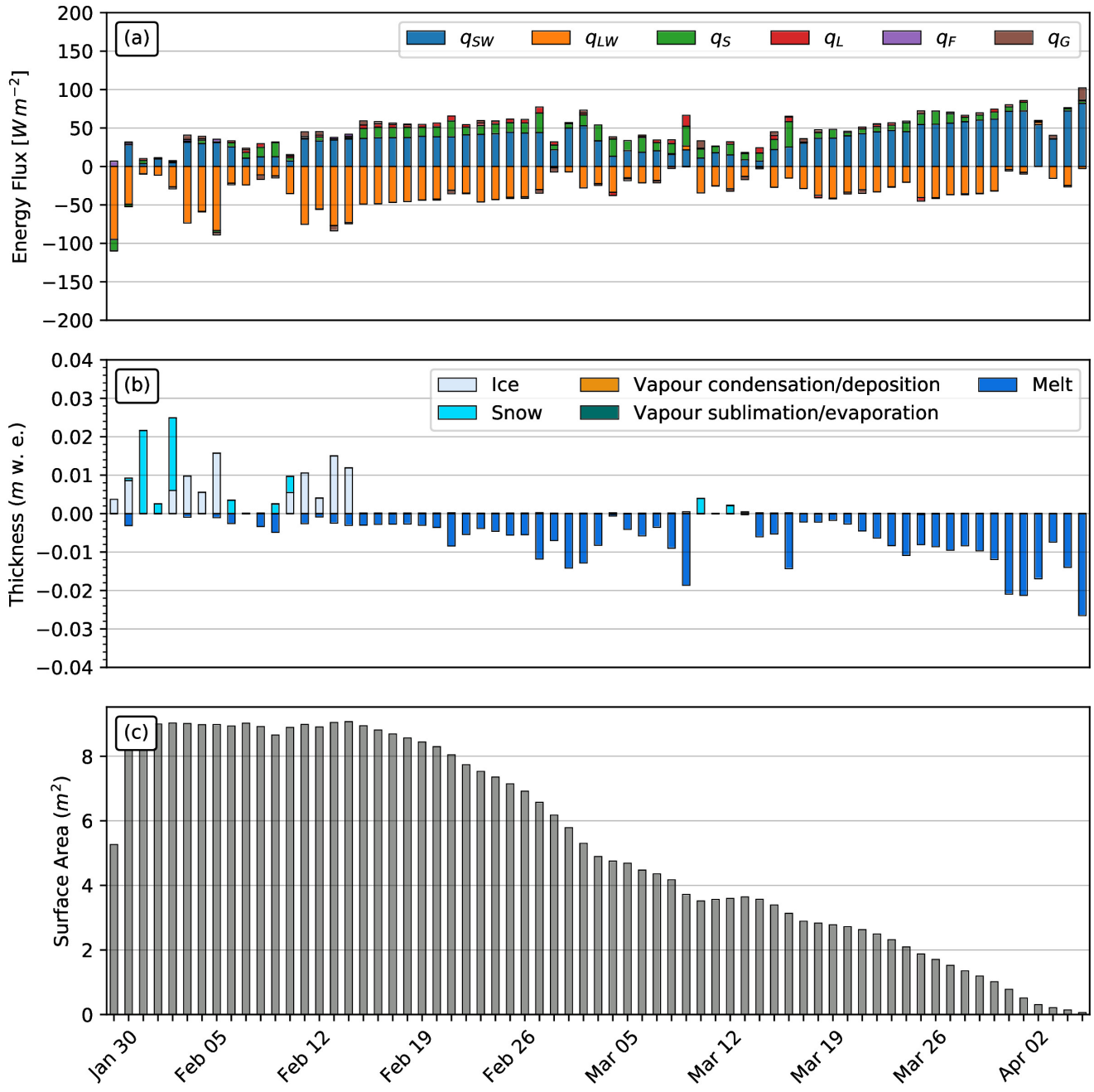


Figure 6. (a) Energy flux components, (b) mass flux components and (c) surface area of the Icestupa in daily time steps. q_{SW} is the net shortwave radiation; q_{LW} is the net longwave radiation; q_L and q_S are the turbulent latent and sensible heat fluxes. q_F represents the interactions of the ice-water boundary during fountain on time steps. q_G quantifies the heat conduction process between the Icestupa surface layer and the ice body.

293 Net shortwave radiation is the main input to, and the most varying energy flux on the ice surface. Its
 294 variability is controlled by the surface albedo α and the area fraction f_{cone} which therefore represent key
 295 variables in the energy balance (Fig. 7 (a)). Although global radiation flux reached a daily maximum value
 296 of $304 W m^{-2}$, q_{SW} only went up to $68 W m^{-2}$. This is caused by the fact that only about 30 percent of
 297 the direct solar radiation influenced the Icestupa surface as shown by the area fraction f_{cone} in Fig. 7 (a).

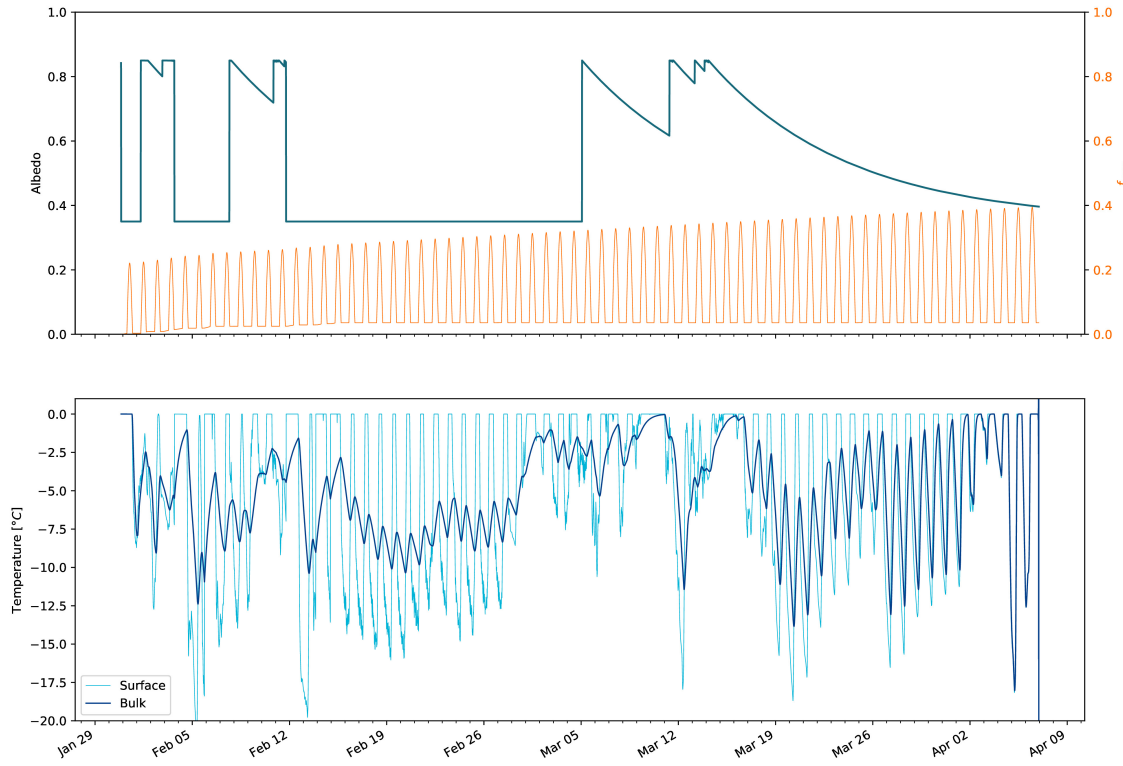


Figure 7. Some derived parameters of the model, namely, albedo and f_{cone} (a), Surface and bulk temperature (b). In (a), the black curve shows how snow and fountain-on events reset albedo between ice albedo and snow albedo. The decay of the snow albedo to ice albedo can also be observed. The blue curve shows how the solar radiation area fraction varied diurnally with variations in the solar elevation angle. In (b), the surface temperature (black curve) was forced to be 0 °C during fountain activity. The corresponding bulk temperature is shown with the blue curve.

298 Snowfall is the atmospheric variable connected most closely and proportionally to albedo. Higher and/or
299 more frequent snowfall thus decreases the energy available for melt due to the corresponding increase in α .

300 q_{LW} was predominantly negative indicating that this energy balance component drove the freezing of the
301 ice structure. The incoming longwave radiation was strongly dependent on atmospheric emissivity which
302 had a mean value of 0.77. Atmospheric emissivity in turn depended on the cloudiness factor. Daily values
303 of q_{LW} ranged from -95 to 7 Wm^{-2} . q_{LW} and q_S were both proportional to the temperature gradient
304 between the air and the Icestupa surface. Turbulent sensible heat flux q_S contributed mostly to the melt
305 of the ice structure. Daily values of q_S ranged from -16 to 59 Wm^{-2} . Turbulent latent heat flux q_L was
306 predominantly positive suggesting that it favoured deposition/condensation over evaporation/sublimation.
307 Daily values of q_L ranged from -4 to 47 Wm^{-2} . Therefore, the Icestupa gained mass cumulatively from
308 the atmosphere due to the deposition/condensation process. Fountain water heat flux q_F had a mean of
309 zero as it was only nonzero during 1002 time steps or around 100 hours. Daily values of q_F ranged from
310 0 to 7 Wm^{-2} . The contribution of heat flux by conduction q_G was minimal as it only varied between
311 -7 to 7 Wm^{-2} with a mean of 0 Wm^{-2} . The energy contributing to surface temperature changes (q_T)
312 was insignificant in comparison to the energy spent on freezing and melting (q_{melt}). The resulting bulk
313 temperature and the surface temperature are shown in Fig. 7 (b). For the total considered period, q_{LW}
314 accounted for 28.3% of overall energy turnover. The energy turnover is calculated as the sum of energy

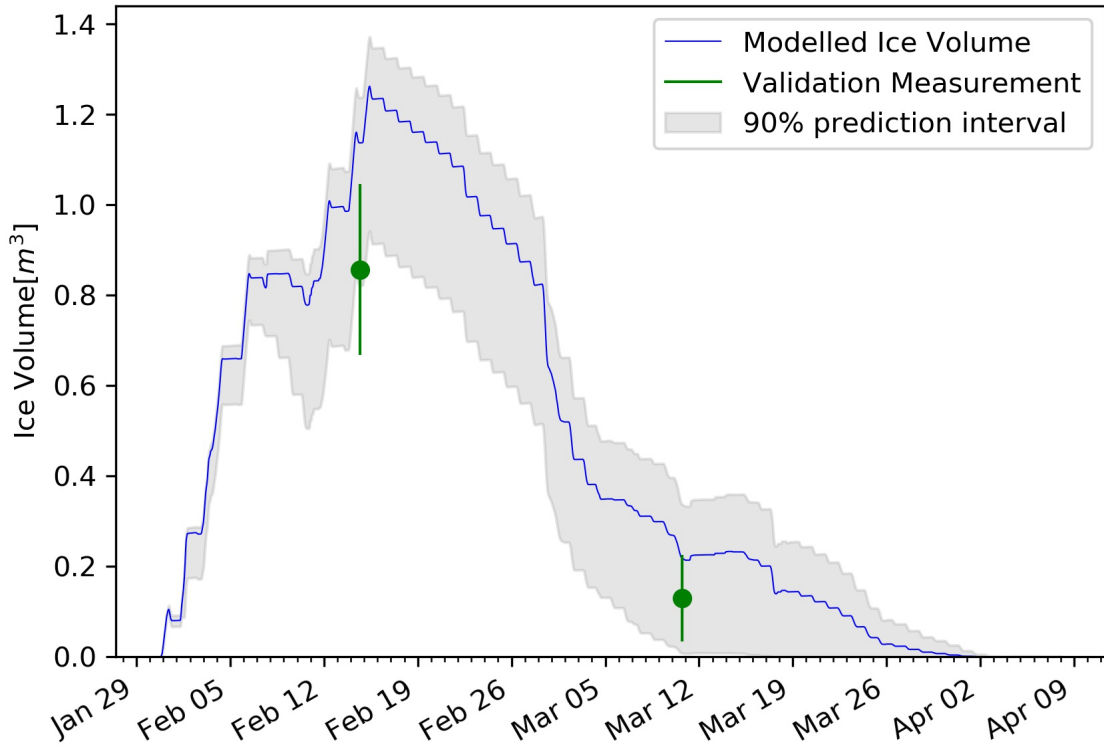


Figure 8. Modelled ice volume during the lifetime of the Schwarzsee Icestupa (blue curve). Green line segments indicate the first and second validation measurements. The prediction interval is based on the ice volume uncertainty caused by the most sensitive parameters, namely, temperature threshold below which precipitation falls as snow and the ice emissivity.

315 fluxes in absolute values. q_{SW} accounted for 21.7%, followed by q_{melt} (25.4%), q_S (14.6%), q_L (7.5%), q_G
316 (1.8%), q_F (0.3%) and q_T (0.3%).

317 Fig. 6 (b) represents the mass fluxes associated with these energy exchanges expressed in m w.e. It
318 shows the ice and meltwater formed due to q_{melt} , snow accumulated due to precipitation, water vapour
319 deposition/condensation and sublimation/evaporation due to q_L . Growth rate ($\frac{\Delta M_{ice}}{\Delta t}$) shows a strong
320 correlation with net energy flux ($r^2 = 0.44$) but poor correlation with Icestupa surface area ($r^2 = 0.04$).
321 This is because the variance in growth rate is mostly due to the variance in q_{net} as illustrated in Fig. 6.
322 Since r_{ice} was initialised with the spray radius r_F , the surface area maintains a maximum initially until the
323 energy flux becomes positive. This trend favours the positive over the negative thickness changes resulting
324 in a steep increase and gradual melting of ice volume as can be seen in Fig. 8.

325 The total water used for the Icestupa development includes contributions from the fountain (97.2%),
326 snowfall (2.5 %) and deposition/condensation (0.3 %) as shown in Table 2. The maximum ice mass during
327 the whole measurement period was 1158 kg, which occurred after the last fountain run on Feb 16th in the
328 morning. Therefore, in the case of Schwarzsee we used a water input of 18,584 kg, with a resultant storage
329 efficiency of only 7.5 %.

5 MODEL SENSITIVITY AND UNCERTAINTY ANALYSIS

330 The icestupa model can be regarded as a function $f(x_1, x_2 \dots, x_n) = (y_1, y_2 \dots, y_m)$, where
331 $(x_1, x_2 \dots, x_n)$ are the model parameters and $(y_1, y_2 \dots, y_m)$ are the model outputs. The influence of each

parameter on the output variables of interest were quantified and the most important physical parameters for the subsequent uncertainty analysis were determined. The sensitivity of a parameter x_j is determined by keeping all other parameters $x_i, i \neq j$ fixed at their baseline value and varying x_j within values that are physically plausible.

A sensitivity study on the parameters (listed in Table 1) was performed with the maximum ice volume as the target variable. All the parameters were assumed to be independent of each other with a uniform distribution. This assumption ignores the auto-correlation present among the parameters associated with the albedo parameterisation. The range of uncertain parameters were set based on available literature values or varied $\pm 5\%$ from the base value if no such reference was available. The uncertainty of all the site parameters were caused due to parallax errors during manual measurement. This was quantified with a range of $\pm 1\%$ from the base value. However, it must be kept in mind that, even though intended to be as objective as possible, the selection of a parameter range has a subjective part that influences the results and conclusions obtained in this analysis. The variation of the model outputs y_k is evaluated to quantify the local sensitivities $s_{j,k}$ that are defined here as the 95% range of the simulated outputs.

To perform the uncertainty analysis, we included only parameters that influence the maximum ice volume by at least $0.1m^3$. All other parameters were fixed at their baseline value. Fig. 9 shows all the variance produced by these uncertain parameters in maximum ice volume calculation. It shows that ϵ_{ice} and T_{train} are the only parameters with a maximal sensitivity of more than $0.1 m^3$ for the maximum ice volume estimate. Consequently, all other parameters were excluded from the subsequent uncertainty analysis.

The temperature threshold below which precipitation falls as snow (T_{train}) was found to be the most sensitive parameter. It is used in the model to reset the albedo to snow albedo and determine snow precipitation events. The lower T_{train} parameter the higher the albedo (as the Icestupa surface has a lower albedo when ice-covered than when snow-covered). The variation of T_{train} by 5% caused maximum ice volume variation of $1.2 \pm 0.2m^3$.

Ice emissivity was also found to be a sensitive parameter. The higher the ice emissivity the larger the maximum ice volume as the emitted longwave radiation increases with ice emissivity. Variation of ϵ_{ice} by 5% caused a maximum ice volume range from $1.3 \pm 0.1m^3$.

In total, the sensitivity analysis required 120 simulations, and the uncertainty analysis a total of 32 simulations.

6 DISCUSSION

6.1 Model validation quality

We first evaluate the model against the validation measurements at the Schwarzsee site. The uncalibrated model is able to capture both the freezing and the melting process sufficiently well as the modelled ice volume lies within the uncertainty of both validation measurements. Furthermore, the validation measurements fit well within the estimated model uncertainty. However, since this validation is based on only two points, it does limit the confidence in the model results. Moreover, the model seems to overestimate the ice volume at both validation points. This could be due to the underestimation of the surface area which underestimates the melt rates (absolute growth rate when $\frac{\Delta M_F}{\Delta t} < 0$) and the freeze rates (absolute growth rate when $\frac{\Delta M_F}{\Delta t} > 0$). However, as the fountain was mostly inactive during the study period, the underestimation of surface area disproportionately undervalues the melt rates over the freeze rates. One major cause of this underestimation was the conical shape assumption, as in reality, the Icestupa shape ranged between a cone and a cylinder (Fig. 2). Another cause was the surface irregularities that

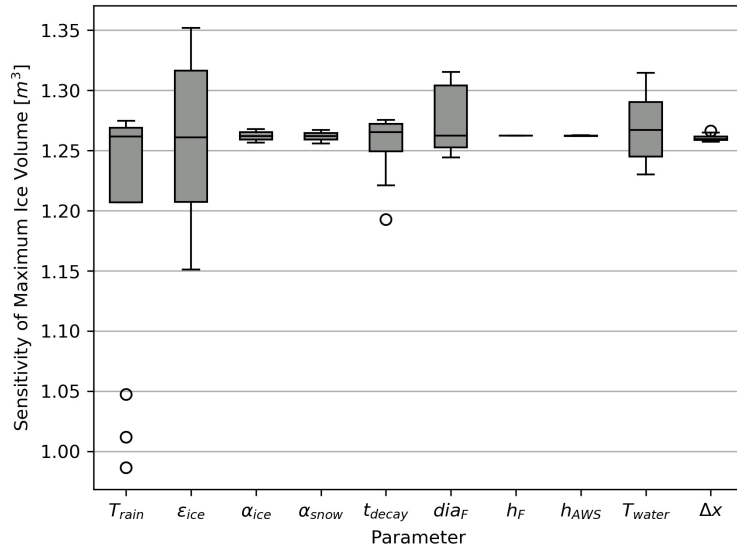


Figure 9. Sensitivities of maximum ice volume to all the uncertain and site parameters used in the model (Table 1). Outliers in the bar plot are shown as 'o'.

were observed due to uneven exposure to direct solar radiation and fountain droplets. The sensitivity of the model results to these errors was further amplified due to the relatively small volume of the Schwarzsee Icestupa. In summary, more validation measurements on a more voluminous Icestupa would have increased confidence on the model results.

6.2 Important assumptions

In the sensitivity and uncertainty analysis presented above, we did not account for several general assumptions and parametrisation choices that may cause model errors. Some assumptions and their potential to cause errors are discussed below.

- Turbulent Sensible and Latent Heat Fluxes: The method used to calculate the turbulent heat fluxes by Garratt (1992) assumes that the turbulent heat fluxes are acting over a uniform planar surface to determine the roughness length. Since our application is on a conical surface, z_{ice} has no real physical significance.
- Droplet flight time loss: Water losses during the flight time of fountain droplets were neglected making all the fountain spray available for freezing. For the Schwarzsee experiment, inclusion of this parameter does not influence results since it is already accounted for in the drained water discharge rate which was at least 3 l min^{-1} .
- Nucleation of droplets: Corresponding to droplet flight time, ice/snow formation is also possible before surface contact if nucleation occurs during flight time. For the Schwarzsee experiment, this process will further increase the freeze rate and hence the storage efficiency. This process is neglected for model simplicity.

6.3 Schwarzsee vs Ladakh Icestupa

It could be argued that the relatively small Schwarzsee Icestupa cannot be compared with the much larger Icestupas in Ladakh which store millions of litres of water for several months (see Appendix 8.1). However, this is the only Icestupa dataset available for such a model validation.

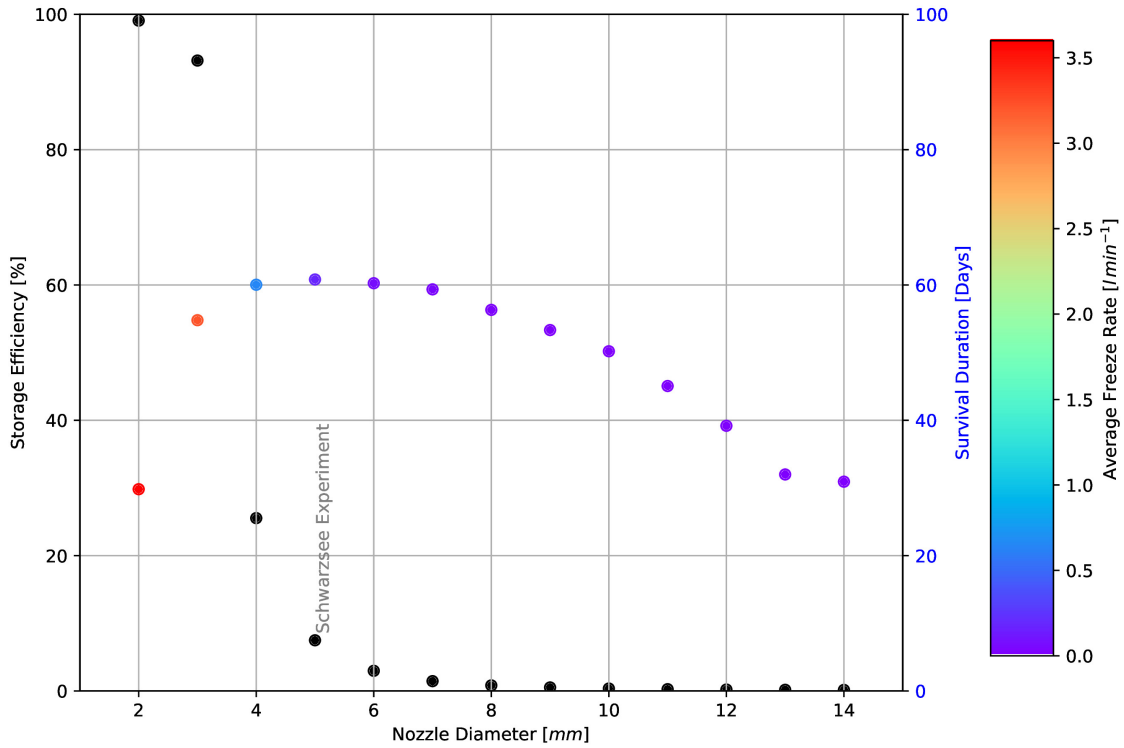


Figure 10. Variation in storage efficiency (black dots) and storage duration (coloured dots) with changes in fountain nozzle's nozzle diameter. The dot colours represent average freeze rate based on the color bar.

397 Table 2 clearly shows that for our Schwarzsee experiment most of the input water (92 %) simply drained
 398 away. This high water loss through drainage is due to the fact that the average spray rate of the fountain
 399 ($(\frac{\Delta \dot{M}_F}{\Delta t})_{mean} = 3.6 l min^{-1}$) far exceeded the max Icestupa growth rate ($(\frac{\Delta M_{ice}}{\Delta t})_{max} = 1 l min^{-1}$ (w.e.)).

400 In the city of Leh, Ladakh at an altitude of 3500 m a.s.l. the air temperature shows values down to
 401 27.9 °C in winter (Chevuturi et al., 2018) whereas Schwarzsee had a minimum temperature of just -11.6
 402 °C during the study period. Moreover, subzero temperatures were only reached for 7 nights of fountain
 403 operation at the Schwarzsee site compared to the 43 nights of fountain operation possible in Ladakh (see
 404 Appendix 8.1). Thus, the Icestupa growth rate is expected to be much higher in Ladakh. However, water
 405 spray rates in Ladakh are also much higher (around $210 l min^{-1}$). So the water losses in Ladakh could
 406 also be caused due to excessive fountain spray.

407 6.4 Icestupa construction decisions

408 There are several decisions one has to take when constructing Icestupas. These can be broadly divided
 409 into two types of decisions, namely fountain and location decisions. Both the meteorological conditions
 410 of the location and the surface area produced by the fountain significantly influence the observed growth
 411 rate. Since our validation is restricted to just one location, we restrict our discussion to the optimization
 412 possibilities of Icestupa constructions through fountain decisions.

413 Assuming a constant spray for the fountain, we can divide the fountain decisions into fountain state
 414 (on/off) and type (height and nozzle diameter). From an energy balance point of view, the fountain should
 415 be switched on for all time intervals when $q_{net} < 0$. However, in our experiment, the fountain state decision
 416 was set based on whether the ambient temperature was above or below a critical temperature of $-5^{\circ}C$.
 417 Ambient temperature can serve as an indicator of q_{net} as it was correlated ($r^2 = 0.53$). However, q_{net}

418 was found to be negative already at a critical temperature of -1°C . Therefore, using air temperature to
419 determine when the fountain should be switched on is justified but a higher critical temperature could have
420 been used in the case of the Schwarzsee Icestupa.

421 The fountain type used can be characterised by the physical structure of the fountain, namely its height and
422 nozzle diameter. Maintaining the same spray rate and height, one can optimize the Icestupa development
423 by identifying the minimum nozzle diameter that yields the maximum storage efficiency.

424 Fig. 10 shows reducing the nozzle diameter to 3 mm increases storage efficiency up to 93 % without
425 compromising much on storage duration. The corresponding storage quantity of the 3 mm nozzle diameter
426 was more than 20 times higher than the 5 mm fountain used in our experiment. This is because the spray
427 radius r_F of the 3 mm fountain was much higher at 8.5 m compared to the 1.7 m spray radius of the
428 5 mm fountain (see Appendix Section ??). Here, we define growth rate as freeze rate when fountain is
429 active and melt rate otherwise. So this higher spray radius both, increases the freeze rate and increases
430 the melt rate since they are both directly proportional to the surface area. However, since the freeze rate
431 cannot increase beyond a spray rate of 3.6 l min^{-1} (except during precipitation or deposition/condensation
432 events), an optimum spray radius or nozzle diameter exists, beyond which storage duration suffers due to a
433 disproportionate increase in melt rate compared to the freeze rate. So even though 3 mm nozzle diameter
434 had a much higher storage quantity than the 5 mm nozzle, its storage duration was around 6 days lesser
435 than the 5 mm nozzle. One physical cause of this effect is the different shapes of both the ice structures. A
436 flat sheet of ice (effectively a cone with a high spray radius) with higher mass might have a storage duration
437 shorter than a conical ice structure. As the spray radius decreases with increasing nozzle diameter, the ice
438 structure's average slope increases and so the 5 mm nozzle's ice structure is "more" conical than the 3 mm
439 ice structure. Fig. 10 shows that a nozzle diameter of 3 mm has an average freeze rate ($3.2\text{ l min}^{-1}\text{w.e.}$)
440 which is large enough to increase the storage efficiency and small enough to not reduce the storage duration
441 of the Icestupa significantly.

7 CONCLUSIONS

442 We outlined a methodology for estimating ice, liquid water, water vapour and drained quantities produced
443 during the construction of an Icestupa using measurements of fountain spray rate, air temperature, radiation,
444 humidity, pressure, wind and cloudiness at the Schwarzsee study site. The comparison with validation
445 measurements at two different dates during the experiment led to satisfying results, although a more
446 rigorous model validation was not possible due to few icestupa volume measurements.

447 According to the model, the Schwarzsee Icestupa achieved a storage quantity of 1392 litres of water with
448 a storage duration of 61 days. However, the corresponding storage efficiency was very low with only 7.5 %
449 for a water input of 18,584 litres. These estimates were most sensitive to the temperature threshold that
450 determined precipitation phase and ice emissivity parameters which created an uncertainty of $1.2 \pm 0.3\text{ m}^3$
451 in the maximum ice volume calculated. This is to be expected as net longwave radiation and net shortwave
452 radiation together accounted for around 50 % of the overall energy turnover.

453 Although the location, storage quantity and duration of our experimental Schwarzsee Icestupa are not
454 representative of the much larger Icestupas of Ladakh, the model results do support the hypothesis that
455 there could be considerable water loss during the formation of Icestupas particularly due to excessive
456 fountain spray. Using model calculations, it was shown that a decreased fountain nozzle diameter of 3 mm
457 can increase the storage efficiency drastically. This is because a change in the fountain nozzle diameter
458 causes an effective change of the ice surface area over which the net energy flux can act. This result has
459 relevance on the future design of Icestupa fountains. However, care has to be taken as our model is currently

460 only validated by one experiment at the Schwarzsee site. Further experiments at different locations with
461 different fountains are required to better understand the influence of construction decisions on the results.

8 APPENDIX

462 8.1 Ladakh Icestupa 2014/15

463 A 20 m tall Icestupa (Wangchuk, 2015c) was built in Phyang village, Ladakh at an altitude of 3500
464 m a.s.l. Assuming a conical shape with a diameter of 20 m, the corresponding volume of this Icestupa
465 becomes 2093 m^3 or 1,919,587 litres w.e. The fountain sprayed water at a rate of 3.5 l s^{-1} (Wangchuk,
466 2015e) from 21st January (Wangchuk, 2015a) to at least until 5th March 2015 (Wangchuk, 2015b) (around
467 43 nights). Assuming fountain spray was active for 8 hours each night, we estimate water consumption to
468 be around 4,334,400 litres. So just during construction/freezing period of the Icestupa, roughly 56 % of the
469 water provided was wasted. The actual water loss is bound to be much higher due to further vapour losses
470 during the melting period. This Icestupa completely melted away on 6th July 2015 (Wangchuk, 2015d).
471 Therefore, the storage duration was 166 days or roughly 5 months.

CONFLICT OF INTEREST STATEMENT

472 The authors declare that the research was conducted in the absence of any commercial or financial
473 relationships that could be construed as a potential conflict of interest.

AUTHOR CONTRIBUTIONS

474 SB wrote the initial version of the manuscript. MH, ML, SW, JO, and FK commented on the initial
475 manuscript and helped improve it. SB developed the methodology with inputs from MH. SB performed the
476 analysis with support from MH and ML. SB and MH participated in the fieldwork.

FUNDING

477 This work was supported and funded by the University of Fribourg and by the Swiss Government Excellence
478 Scholarship (Suryanarayanan Balasubramanian).

ACKNOWLEDGMENTS

479 We thank Mr. Adolf Kaeser and Mr. Flavio Catillaz at Eispalast Schwarzsee for their active participation
480 in the fieldwork. We would also like to thank Digmesa AG for subsidising their flowmeter used in the
481 experiment. We would particularly like to thank the editor Prof. Thomas Schuler who gave us important
482 inputs to improve the paper and we thank also Prof. Christian Hauck and Prof. Nanna B. Karlsson for
483 valuable suggestions that improved the manuscript.

DATA AVAILABILITY STATEMENT

484 The data and code used to produce results and figures will be published at a later stage and can, until then,
485 be obtained from the authors upon request.

REFERENCES

- 486 Apel, H., Abdykerimova, Z., Agalhanova, M., Baimaganbetov, A., Gavrilenko, N., Gerlitz, L., et al. (2018).
487 Statistical forecast of seasonal discharge in central asia using observational records: development of a
488 generic linear modelling tool for operational water resource management. *Hydrology and Earth System*
489 *Sciences* 22, 2225–2254. doi:10.5194/hess-22-2225-2018

- 490 Bonales, L. J., Rodriguez, A. C., and Sanz, P. D. (2017). Thermal conductivity of ice prepared under
491 different conditions. *International Journal of Food Properties* 20, 610–619. doi:10.1080/10942912.
492 2017.1306551
- 493 Brutsaert, W. (1975). On a derivable formula for long-wave radiation from clear skies. *Water Resources
494 Research* 11, 742–744. doi:10.1029/WR011i005p00742
- 495 Brutsaert, W. (1982). *Evaporation into the Atmosphere. Theory, History and Application* (Kluwer Academic
496 Publishers)
- 497 Buck, A. L. (1981). New equations for computing vapor pressure and enhancement factor. *Journal of
498 Applied Meteorology and Climatology* 20, 1527 – 1532
- 499 Buytaert, W., Moulds, S., Acosta, L., Bievre, B. D., Olmos, C., Villacis, M., et al. (2017). Glacial melt
500 content of water use in the tropical andes. *Environmental Research Letters* 12, 114014. doi:10.1088/
501 1748-9326/aa926c
- 502 Chen, Y., Li, W., Deng, H., Fang, G., and Li, Z. (2016). Changes in central asia's water tower: Past, present
503 and future. *Nature* doi:10.1088/1748-9326/aa926c
- 504 Chevuturi, A., Dimri, A. P., and Thayyen, R. J. (2018). Climate change over leh (ladakh), india. *Theoretical
505 and Applied Climatology* 131, 531–545. doi:10.1007/s00704-016-1989-1
- 506 [Dataset] Copernicus Climate Change Service (C3S) (2017). Era5: Fifth generation of ecmwf atmospheric
507 reanalyses of the global climate
- 508 Cuffey, K. M. and Paterson, W. S. B. (2010). *The Physics Of Glaciers* (Elsevier)
- 509 Fujita, K. and Ageta, Y. (2000). Effect of summer accumulation on glacier mass balance on the
510 tibetan plateau revealed by mass-balance model. *Journal of Glaciology* 46, 244–252. doi:10.3189/
511 172756500781832945
- 512 Garratt, J. R. (1992). *The Atmospheric Boundary Layer* (Cambridge University Press)
- 513 Grossman, D. (2015). As himalayan glaciers melt, two towns face the fallout
- 514 Hersbach, H., Bell, B., Berrisford, P., Hirahara, S., Horányi, A., Muñoz-Sabater, J., et al. (2020). The era5
515 global reanalysis. *Quarterly Journal of the Royal Meteorological Society* 146, 1999–2049
- 516 Hock, R., Rasul, G., Adler, C., Cáceres, B., Gruber, S., Hirabayashi, Y., et al. (2019). 2019: High mountain
517 areas. *IPCC Special Report on the Ocean and Cryosphere in a Changing Climate* [H.-O. Pörtner, D.C.
518 Roberts, V. Masson-Delmotte, P. Zhai, M. Tignor, E. Poloczanska, K. Mintenbeck, A. Alegria, M. Nicolai,
519 A. Okem, J. Petzold, B. Rama, N.M. Weyer (eds.)]
- 520 Hoelzle, M., Barandun, M., Bolch, T., Fiddes, J., Gafurov, A., Muccione, V., et al. (2019). *The status and
521 role of the alpine cryosphere in Central Asia*. doi:10.4324/9780429436475-8
- 522 [Dataset] IDAWEB (2019). Meteoswiss, federal office of meteorology and climatology
- 523 Immerzeel, W. W., Lutz, A. F., Andrade, M., Bahl, A., Biemans, H., Bolch, T., et al. (2019). Importance
524 and vulnerability of the world's water towers. *Nature* 577, 364 – 369. doi:10.1038/s41586-019-1822-y
- 525 Meteoblue (2020). Climate schwarzsee
- 526 Mölg, T. and Hardy, D. R. (2004). Ablation and associated energy balance of a horizontal glacier surface
527 on kilimanjaro. *J. Geophys. Res.-Atmos.* 109, 1–13. doi:10.1029/2003JD004338
- 528 Nüsser, M., Dame, J., Kraus, B., Baghel, R., and Schmidt, S. (2019a). Socio-hydrology of artificial glaciers
529 in ladakh, india: assessing adaptive strategies in a changing cryosphere. *Regional Environmental Change*
530 doi:10.1007/s10113-018-1372-0
- 531 Nüsser, M., Dame, J., Parveen, S., Kraus, B., Baghel, R., and Schmidt, S. (2019b). Cryosphere-Fed
532 Irrigation Networks in the Northwestern Himalaya: Precarious Livelihoods and Adaptation Strategies
533 Under the Impact of Climate Change. *Mountain Research and Development* 39. doi:10.1659/
534 MRD-JOURNAL-D-18-00072.1

- 535 Oerlemans, J. and Knap, W. H. (1998). A 1 year record of global radiation and albedo in the
536 ablation zone of morteratschgletscher, switzerland. *Journal of Glaciology* 44, 231–238. doi:10.
537 3189/S0022143000002574
- 538 Schmidt, L. S., Aðalgeirsdóttir, G., Guðmundsson, S., Langen, P. L., Pálsson, F., Mottram, R., et al. (2017).
539 The importance of accurate glacier albedo for estimates of surface mass balance on vatnajökull: evaluating
540 the surface energy budget in a regional climate model with automatic weather station observations. *The
541 Cryosphere* 11, 1665–1684. doi:10.5194/tc-11-1665-2017
- 542 Stigter, E. E., Litt, M., Steiner, J. F., Bonekamp, P. N. J., Shea, J. M., Bierkens, M. F. P., et al. (2018).
543 The importance of snow sublimation on a himalayan glacier. *Frontiers in Earth Science* 6, 108.
544 doi:10.3389/feart.2018.00108
- 545 Tetens, O. (1930). Über einige meteorologische begriffe. z. *Geophys.* 6, 297–309
- 546 Unger-Shayesteh, K., Vorogushyn, S., Farinotti, D., Gafurov, A., Duethmann, D., Mandychev, A., et al.
547 (2013). What do we know about past changes in the water cycle of central asian headwaters? a review.
548 *Global and Planetary Change* 110, 4 – 25. doi:10.1016/j.gloplacha.2013.02.004. Water in Central Asia
549 – Perspectives under global change
- 550 Wangchuk, S. (2014). Ice stupa artificial glaciers of ladakh
- 551 Wangchuk, S. (2015a). The good news at ice stupa 24th january 2015
- 552 Wangchuk, S. (2015b). Ice stupa artificial glacier inaugurated 5th of march 2015
- 553 Wangchuk, S. (2015c). Ice stupa surpasses guiness world record
- 554 Wangchuk, S. (2015d). Ice stupa way of celebrating a special day
- 555 Wangchuk, S. (2015e). World water day at ice stupa
- 556 WMO (2018). *Guide to Instruments and Methods of Observation* (World Meteorological Organization ;
557 2018 (2018 Edition))
- 558 Woolf, H. M. (1968). *On the Computation of Solar Elevation Angles and the determination of sunrise and
559 sunset times* (National Aeronautics and Space Administration)
- 560 Zhou, S., Kang, S., Gao, T., and Zhang, G. (2010). Response of zhadang glacier runoff in nam co basin,
561 tibet, to changes in air temperature and precipitation form. *Chinese Science Bulletin* 55, 2103–2110.
562 doi:10.1007/s11434-010-3290-5